AGU PUBLICATIONS

JGR

Journal of Geophysical Research: Earth Surface

RESEARCH ARTICLE
10.1002/2014JF003432

Key Points:
- Detrital thermochronometers record spatial pattern of erosion
- Nearly uniform erosion under the present-day glacier
- The largest observed source area of erosion is near the ELA

Supporting Information:
- Figure S1 and Tables S1–S4

Correspondence to:
T. A. Ehlers,
todd.ehlers@uni-tuebingen.de

Citation:
Ehlers, T. A., A. Szameitat, E. Enkelmann, B. J. Yanites, and G. J. Woodsworth (2015), Identifying spatial variations in glacial catchment erosion with detrital thermochronology, *J. Geophys. Res. Earth Surf.*, *120*, 1023–1039, doi:10.1002/2014JF003432.

Received 31 DEC 2014
Accepted 8 MAY 2015
Accepted article online 12 MAY 2015
Published online 18 JUN 2015

Identifying spatial variations in glacial catchment erosion with detrital thermochronology

Todd A. Ehlers[1], Annika Szameitat[1], Eva Enkelmann[1,2], Brian J. Yanites[1,3,4], and Glenn J. Woodsworth[5]

[1]Department of Geosciences, Universität Tübingen, Tübingen, Germany, [2]Now at Department of Geology, University of Cincinnati, Cincinnati, Ohio, USA, [3]Department of Earth and Environmental Sciences, University of Michigan, Ann Arbor, Michigan, USA, [4]Now at Department of Geological Sciences, Univeristy of Idaho, Moscow, Idaho, USA, [5]Geological Survey of Canada, Vancouver, British Columbia, Canada

Abstract Understanding the spatial distribution of glacial catchment erosion during glaciation has previously proven difficult due to limited access to the glacier bed. Recent advances in detrital thermochronology provide a new technique to quantify the source elevation of sediment. This approach utilizes the tendency of thermochronometer cooling ages to increase with elevation and provides a sediment tracer for the elevation of erosion. We apply this technique to the Tiedeman Glacier in the heavily glaciated Mount Waddington region, British Columbia. A total of 106 detrital apatite (U-Th)/He (AHe) and 100 apatite fission track (AFT) single-grain ages was presented from the modern outwash of the Tiedemann Glacier with catchment elevations between 530 and 3960 m. These data are combined with nine AHe and nine AFT bedrock ages collected from a ~2400 m vertical transect to test the hypotheses that erosion is uniformly or nonuniformly distributed in the catchment. A Monte Carlo sampling model and Kuiper statistical test are used to quantify the elevation range where outwash sediment is sourced. Model results from the AHe data suggest nearly uniform erosion in the catchment, with a preference for sediment being sourced from ~2900 to 2700 m elevation. Ages indicated that the largest source of sediment is near the present-day ELA. These results demonstrate the utility of AHe detrital thermochronology (and to a lesser degree AFT data) to quantify the distribution of erosion by individual geomorphic processes, as well as some of the limitations of the technique.

1. Introduction

It has long been acknowledged that alpine glacial erosion is an effective agent of erosion and is responsible for an increase in erosion over the last 2 Ma [e.g., *Herman et al.*, 2013]. However, a limited number of observational and modeling studies have quantified glacial erosion processes at the catchment scale [e.g., *Hallet et al.*, 1996; *Braun et al.*, 1999; *Berger et al.*, 2008; *Herman and Braun*, 2008; *Egholm et al.*, 2009; *Yanites and Ehlers*, 2012]. With a few exceptions, rigorous observational studies of glacial erosion have been hampered by the overlying ice that obscures access to the actively eroding bed. Previous work [e.g., *Hallet et al.*, 1996, and references therein] has documented sediment fluxes from modern glaciers and thicknesses of glacially deposited sediment. These studies provide insight into the magnitude of erosion at the catchment scale, but little information about the spatial distribution of erosion within a glaciated catchment. In the last decade, advances in thermochronology have enabled a new approach to address such problems. In particular, the measurement of individual thermochronometric ages from a sediment sample (i.e., detrital thermochronology) offers a new tool to track the elevation where eroded sediment originated [e.g., *Hurford and Carter*, 1991; *Carter*, 1999; *Spiegel et al.*, 2004; *Kuhlemann et al.*, 2005; *Carrapa et al.*, 2006; *Stock et al.*, 2006; *Vermeesch*, 2007; *Avdeev et al.*, 2011] as well as tectonic processes [*Brewer et al.*, 2003; *Ruhl and Hodges*, 2005; *Reiners et al.*, 2007; *Whipp et al.*, 2009; *Enkelmann et al.*, 2009; *Tranel et al.*, 2011]. In this study we measure detrital thermochronometer cooling ages from glacial outwash sediment sourced from a modern glacier to quantify the spatial distribution of erosion within the catchment.

Previous detrital thermochronometer studies were typically conducted using thermochronometer systems sensitive to high closure temperatures that range from 90 to 120°C [*Green et al.*, 1986; *Carlson et al.*, 1999] for apatite fission track (AFT) to ~350–400°C for $^{40}Ar/^{39}Ar$ on biotite [*McDougall and Harrison*, 1999, and references therein]. The lower temperature apatite (U/Th)-He (AHe) system has a closure temperature of ~70°C [*Farley*, 2002] and provides a way of quantifying processes that occur much closer to the Earth's surface. Regardless of the thermochronometer system used, the utility of using detrital thermochronology

as a tracer of the elevation that sediment came from relies on having a well-defined bedrock age-elevation relationship with a large range of ages. This criterion is met for previous studies from the Sierra Nevada and White Mountains, USA [*Stock et al*., 2006; *Vermeesch*, 2007]. Our application of detrital thermochronology in this study quantifies that the elevation sediment is sourced from bedrock but is not sensitive to the duration of time that sediment is transported through the glacial system. The AHe system has a low closure temperature that records the most recent cooling history of the catchment. As such, it more likely records recent glacial erosion to a higher fidelity than other chronometers that may also contain cooling information related to older erosion processes and events or even igneous intrusions. The disadvantage to the AHe system is that closure temperature depths are typically shallow (2–3 km depth) where topographic bending of isotherms [*Stüwe et al*., 1994] can cause scatter in the age-elevation relationship [e.g., *Ehlers and Farley*, 2003]. With few exceptions, a limited number of studies have so far applied detrital thermochronology data from AHe dating to address orogen erosion and surface processes [*Stock et al*., 2006; *Reiners et al*., 2007; *Vermeesch et al*., 2009; *Tranel et al*., 2011; *McPhillips and Brandon*, 2010].

This study compliments previous work by quantifying the distribution of glacial erosion from AHe and AFT data collected from the modern outwash of an active glacier. In doing this, we test the hypothesis that the distribution of erosion in a glacial catchment is nonuniform and preferentially focused near the equilibrium line altitude (ELA). We apply these techniques to the Tiedemann Glacier, located in the heavily glaciated Mount Waddington region of British Columbia. A total of 106 detrital and 9 bedrock single-grain AHe ages is presented and combined with 100 detrital AFT ages and 9 bedrock AFT ages of the same samples. These data are interpreted with a Monte Carlo model to quantify the spatial distribution of erosion within the catchment. Furthermore, the limitations and caveats associated with this technique are discussed.

2. Background to Detrital Thermochronology on Glacial Sediments

Detrital thermochronology offers a relatively new technique to trace the elevations from which sediment is sourced. In the context of glacial settings, this technique has potential to evaluate theoretical predictions for the distribution of erosion within glaciated catchments [e.g., *Braun et al*., 1999; *Egholm et al*., 2009; *Herman and Braun*, 2008; *Yanites and Ehlers*, 2012; *Headley and Ehlers*, 2015]. A comparison to glacial landscape evolution models is beyond the scope of this study, and we instead focus here on introducing how the detrital thermochronometer technique can be applied in glaciated catchments to quantify the distribution of erosion. Future work will emphasize integration with landscape evolution models.

Stock et al. [2006] were the first to use detrital AHe ages to quantify the distribution of catchment erosion by comparing predicted and measured probability density functions (PDFs) to identify uniform versus nonuniform erosion in two adjacent catchments in the Sierra Nevada, California, USA. The approach used is modified from that of *Ruhl and Hodges* [2005] conducted using white mica $^{40}Ar/^{39}Ar$ ages from modern river sediments in the Nepalese Himalaya. There are several considerations involved in the interpretation of detrital ages for the distribution of erosion (Figure 1). For comparison with measured data a predicted (or synthetic) PDF is produced assuming the simplified case of uniform erosion (Figure 1a). The predicted PDF is created from the convolution of the catchment hypsometry upstream of the sample location with a bedrock-derived age-elevation relationship from the catchment. This predicted PDF produces a distribution of ages assuming each location (or pixel) in the digital elevation model (DEM) contributes an equal amount of sediment to the detrital sample location. In the case of uniform erosion every unit area of the catchment is delivering the same amount of sediment and the calculated PDF will have the same shape as the hypsometric curve [*Stock et al*., 2006]. Thus, the probability of delivering sediment from each elevation is proportional to the fractional area of this elevation. A measured distribution of grain ages can then be compared to the predicted PDF using statistical tests described below to test the simplified assumption of uniform erosion.

For a glacial setting the distribution of erosion could be nonuniform and localized, for example, in cirques, at tributary junctions where small glaciers join a larger glacier, and/or near the ELA where sliding velocities can be higher [*Anderson et al*., 2006] (Figure 1b). In these cases, a mismatch in the predicted and observed PDFs can occur. Peaks in the measured PDF can reflect elevations with enhanced erosion as well as the catchment hypsometry (Figure 1c). Because of the ramp like geometry of the Tiedemann Glacier bed and ice surface, no

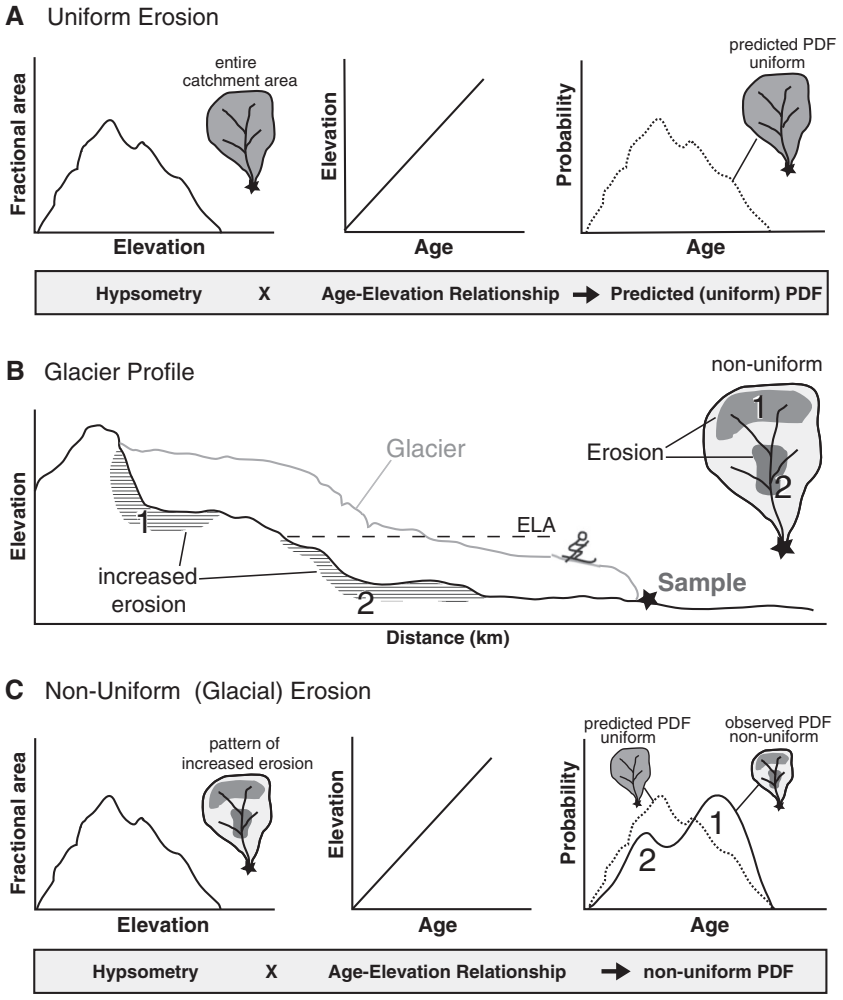

Figure 1. (a) Schematic diagram illustrating how detrital thermochronometer data from outwash or a terminal moraine sediment can be used to quantify the spatial distribution of erosion in a catchment. Simplified approach whereby the convolution of the catchment hypsometry and an age-elevation relationship are used to construct a predicted PDF. This approach assumes a uniform distribution of erosion over the catchment. (b) Glacier profile, showing increased erosion at higher elevations and steps in the slope of the underlying bedrock. (c) Comparison of a predicted PDF for uniform (Figure 1a) and nonuniform (glacial) erosion. Ages (and respective elevations) with increased erosion are clearly visible in the measured PDF when compared to the uniform erosion PDF. In this example, the peaks in measured ages (e.g., 1 and 2) are shifted to older and slightly younger ages when compared to the predicted PDF due to increased erosion at higher elevations (Figures 1a and 1c modified after *Stock et al.* [2006]).

such major peaks are expected in the setting of this study (e.g., see section 4.3 and discussion in Figure 6). The resulting PDF—based on the modeled subice surface—is more likely to show a more or less uniform pattern of erosion with possibly the maximum occurring below the ELA.

3. Geological Setting, Sampling, and Sediment Mixing

The Mount Waddington region of the Coast Mountains, British Columbia, is located on the west coast of Canada, approximately 300 km northwest of Vancouver (Figure 2). The geological history of British Columbia is characterized by the accretion of multiple terranes during the Mesozoic and the metamorphism and partial melting of rocks associated with these collisions. During and after the accretion of the terranes from the Middle Jurassic through the Eocene numerous intrusions and volcanic complexes formed due to subduction-related volcanism. Since then, the region has experienced only limited magmatic activity inland of the plate boundary. Steady surface uplift of up to 3.5 km occurred over the last 40 Ma, first in the northern

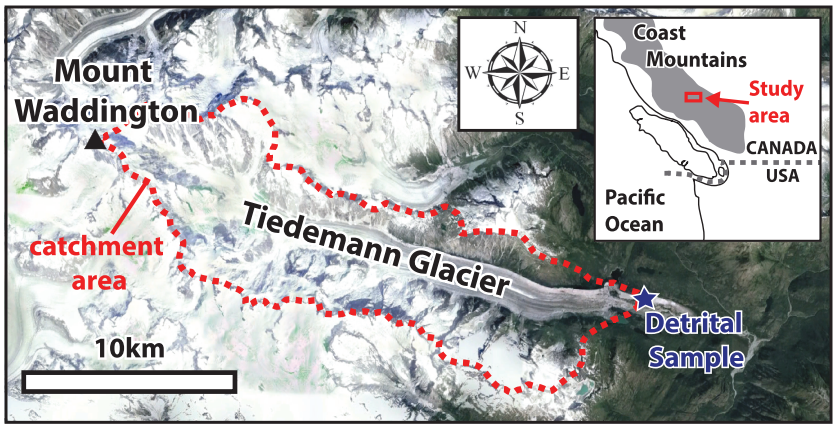

Figure 2. Location of study area in southern Coast Mountains, British Columbia, Canada (images from Google Earth).

regions during the late Miocene and later after the end of the major volcanic phase during the Pleistocene and Pliocene in the southern Coast Mountains [*Parrish*, 1983]. In the Quaternary the region experienced several phases of glaciation with many glaciers carving U-shaped valleys and producing glacial deposits [*Osborn and Luckman*, 1988]. Numerous climatological and glaciological studies have dated abandoned terminal moraines of the Tiedemann Glacier, which provide us with a detailed picture of the development of this glacier in the last 6000 years [e.g., *Laroque and Smith*, 2003, 2005; *Osborn and Luckman*, 1988].

Our study area along the Tiedemann Glacier is located on the eastern side of Mount Waddington (Figure 2), an area dominated by granodiorite and tonalite intrusions of probable early Tertiary age, orthogneiss of uncertain age, and minor amphibolite facies metamorphic rocks [*Rusmore and Woodsworth*, 1994]. The intrusions and orthogneisses have broadly similar composition, and all bedrock samples have high concentrations of apatite, suggesting a low lithologic bias in apatite sourcing. Thus, the area is well suited for thermochronology studies. Numerous studies [e.g., *Parrish*, 1983; *O'Sullivan and Parrish*, 1995; *Shuster et al.*, 2005; *Ehlers et al.*, 2006; *Densmore et al.*, 2007; *Olen et al.*, 2012] have produced a large data set of bedrock thermochronology data from Mount Waddington and surrounding areas. This detailed knowledge of the exhumation history and the age-elevation relationship of the area make it a well-suited location for a detrital thermochronometer.

The bedrock samples of this study were collected in the drainage area of the glacier over an elevation range of ~2400 m and a total distance of 25 km. In addition to bedrock samples near the toe of the glacier, samples were collected along two vertical profiles (one halfway up the glacier and another near the glacier crest). These samples cover most of the elevation range of the glacier (Figure 3). For the analysis of detrital grains, approximately 10 kg of sediment from the modern outwash channel was collected 300 m downstream of the toe of the glacier immediately adjacent to the channel (photographs provided in the supporting information). To avoid bias in the age distribution, this large quantity was collected as a composite sample of ~30 sample sites along a ~50 m reach of the outwash channel. A small amount of sediment, ranging across grain sizes from glacial flour to ~2 cm diameter small pebbles, was collected every few meters to produce a representative sample of the location. For practical reasons in the field the sample amount was limited to 10 kg. This sample size provided far more apatite than is needed for this study. Clast sizes >2 cm (e.g. cobbles and boulders near the outwash channel or in the proglacial zone) were not sampled and the effect of clast size and transport distance on cooling ages could not be investigated and is a topic needing future investigation.

Glacial catchment processes can produce debris that is both poorly and well mixed. Given this, our assumption that the glacial fluvial outwash sediment sampled in this study is a mixture of sediment produced within the glacier warrants discussion. Different lines of evidence support mixing of glacial sediment that reaches the outwash zone. First, glacial debris can be highly folded and mixed within the glacier itself. Deformation and mechanical mixing of ice and debris have been documented for supraglacial material deposited on ice by valley wall mass wasting onto the glacier, and also medial moraines that are at the time of deposition not well mixed [e.g., *Ward and Anderson*, 2011], but become deformed by the time they reach the glacier terminus [e.g., *Hambrey et al.*, 1999; *Goodsell et al.*, 2005]. These mixing processes occur by deformation of ice during flow down the valley. Complex deformation

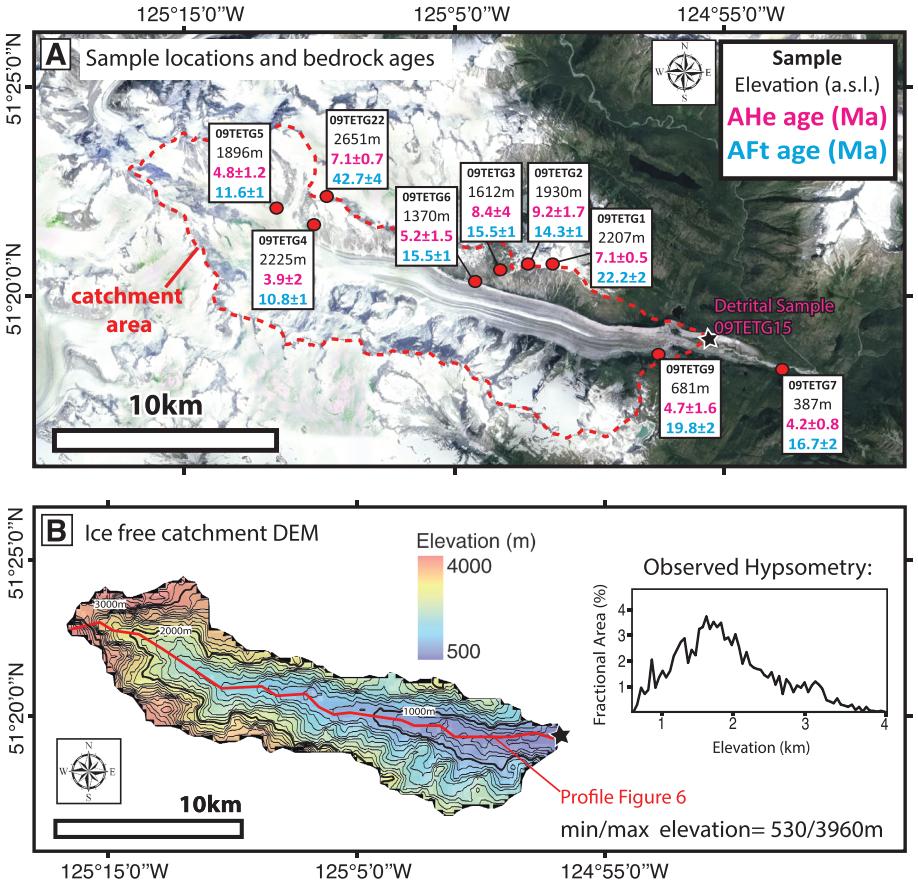

Figure 3. (a) Bedrock sample locations (red dots), elevations (black), and mean bedrock ages for apatite U-Th/He data (pink) and apatite fission track data (blue) along the Tiedemann Glacier. The star marks the location of the detrital sample 09TETG015 (background image by Google Earth). (b) Ice-free catchment DEM and resulting hypsometry of the Tiedemann Glacier catchment for the detrital sample (black star) (DEM from *Clarke et al.* [2009]). The red line shows the path of the profile depicted in Figure 6.

structures are preserved within ice and also within basal ice and support our assumption of mechanical mixing [*Goodsell et al.*, 2005]. Second, as deformed ice structures melt, they provide sediment to the subglacial fluvial system that eventually provides sediment to our sample location in the proglacial zone. These sediments are mixed within the glacial fluvial system underneath the ice and when the sediments exit the glacier. Fluvial mixing of sediment is highly efficient during turbulent flow and forms the basis for cosmogenic nuclide studies of catchment denudation rates [e.g., *Schaller et al.*, 2001]. Glacial fluvial sedimentary facies are also formed in the subglacial and proglacial environment and are often stratified and have heterogeneous lithologies [*Menzies and Shilts*, 2002; *Brodzikowski and van Loon*, 1991]. The transfer of sediment to our sample location by melted deformed ice and subglacial fluvial processes suggest that sediment sampled from the outwash channel exiting the glacier is mixed and representative of material entrained in the ice by different processes. Third, our sampling approach included an amalgamation of ~30 sample locations from the proglacial outwash zone to provide a representative sample of this location. Finally, in a parallel study to this one [*Enkelmann and Ehlers*, 2013, also unpublished data, 2015], we sampled the ice-cored ablation zone on the Tiedemann Glacier, about 1.5 km upstream from the glacier terminus where the outwash sample was collected. Five samples from the ablation zone were collected, and a total of 521 detrital AFT ages was measured. When the ablation zone samples are combined, the age distribution is statistically identical to the outwash sample presented in this study. Thus, given the above arguments, the detrital grain ages presented here are at the very least a representative mixture of sediment $>$ ~2 cm across the ablation zone and most likely the upstream glacial catchment that provided the sediment sampled in this study.

4. Methods

Mineral separations of the bedrock and detrital samples were conducted using standard magnetic and heavy-liquid separation techniques. We dated apatites from the modern outwash sediment of the Tiedemann Glacier and from nine bedrock samples from the vertical transect using the AHe and AFT techniques (Figure 3a). The complete data set is shown in Tables S1 and S2 in the supporting information.

4.1. Analytical Methods: Apatite (U-Th)/He Analysis

Apatites with a grain diameter less than 250 μm were picked using a 160X cross-polarized binocular microscope. Most grains had a minimum diameter of 90 μm and were inclusion free to avoid effects of He production from inclusions or excess loss of He during decay due to a large surface/volume ratio [*Farley*, 2000]. Furthermore, nearly all grains in the samples had an euhedral geometry, or broken but nearly complete euhedral grains, rather than well-rounded grains seen in many sedimentary rock samples. The grains were similar in appearance to the moraine sample shown in *Stock et al.* [2006] (see supporting information). The limiting factor for grain selection was grain size and the presence/absence of inclusions rather than the grain shape. The prevalence of euhedral grains in the detrital sample is likely due to the short transport distance (<25 km) in this setting and the production of grains from larger material that is broken down during transport (comminution). Despite our best efforts to minimize any bias in grain selection due to grain quality, the possibly exists that there is a systematic bias in our analysis. Recent work by *Tripathy-Lang et al*. [2013] using zircon (U-Th)/He laser ablation analyses presents a promising new tool to avoid any bias in grain selection by dating the center of randomly selected grains. However, this technique awaits application to apatite, which may prove challenging due to the lower He gas production in this mineral compared to zircon.

The grain dimensions were measured for calculation of the alpha-ejection ($F\tau$) correction [*Farley et al*., 1996]. Following this, single grains were packed in Nb tubes for U, Th, Sm, and He measurement. The ^{4}He concentration was measured on a Patterson Instruments gas extraction line at the University of Tübingen, Germany. Samples were heated for 5 min at 11 Amps with a 960 nm diode laser for degassing. Evolved He was spiked with ^{3}He, and the ^{4}He/^{3}He ratio was measured with a quadrupole mass spectrometer. Each grain was reheated to verify all ^{4}He was extracted by the first heating step. After degassing the U, Th, and Sm were measured after dissolution in HNO_3 and HF and spiking with ^{235}U and ^{230}Th. Uranium, Th, and Sm measurements were conducted using an inductively coupled plasma mass spectrometer at the University of Arizona, Tucson, USA. All grains were dated by single-grain analysis to quantify the reproducibility of bedrock samples, and bedrock ages were later averaged to determine their mean age (Table S1).

For visualization purposes, we generate a probability density function (PDF) based on the measured detrital grain ages (Figure 5). Each detrital grain age is used to generate a continuous normal distribution with a mean of the measured age and a standard deviation based on the reproducibility of the bedrock samples (explained below). The normal distributions of all the detrital grains are normalized by the number of grains and then stacked to generate a PDF of the population. The PDFs were generated following the approach of *Brandon* [1996] with an alpha value of 0.6 to avoid double smoothing of the stacked distributions when calculating the PDF. This results in a PDF that accounts for uncertainty resulting from sample reproducibility. Note that the statistical analysis (Kuiper test) described below compares smoothing corrected PDFs [cf., *Brandon*, 1996].

Determination of the measured cooling age PDF requires knowledge of the bedrock sample reproducibility [e.g., *Stock et al*., 2006] whereby high reproducibility results in high-frequency variations (i.e., jagged appearance) in the PDF and lower reproducibility results in a smoother looking PDF. The analytical uncertainty of the AHe samples presented is that this study is <6% (2σ) for the data in Tables S1 and S2. The total uncertainty also depends on the reproducibility error of the aliquots that are reported in Table S1 and are typically higher than the analytical error. This approach differs from studies of detrital U-Pb or ^{40}Ar/^{39}Ar grain age distributions where the analytical uncertainty is used to create the distribution rather than the bedrock reproducibility (which is often unknown). Because replicate analyses are not possible for detrital samples, we used the averaged uncertainty from seven of our bedrock samples, weighted by the number of grains analyzed of each sample for their contribution to the mean ages. The remaining two

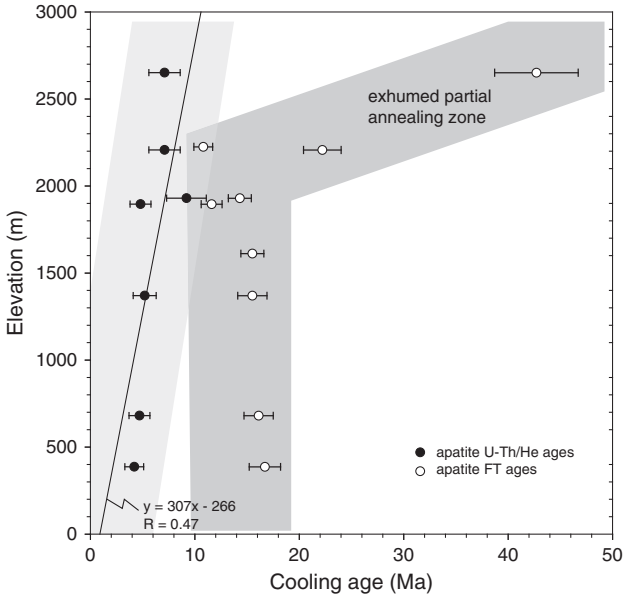

Figure 4. Bedrock cooling ages for apatite U-Th/He ages and apatite fission track ages. The age-elevation relationship equation shown for the apatite U-Th/He data was used in the calculations of the PDFs. The AFT data suggests an exhumed partial annealing zone with rapid uplift starting around 20 Ma.

bedrock samples were excluded due to a high reproducibility error of more than 40% (likely due to He implantation or zoning of U-Th in some aliquots) and/or a low gas yield resulting in an analytical error of more than 6% (Table S1). The resulting mean reproducibility of the bedrock samples is 21%, which were then used as the uncertainty for our detrital AHe ages. This level of reproducibility is lower than previous bedrock AHe analyses from the same lithology on the other (western) side of Mount Waddington [*Ehlers et al.*, 2006; *Densmore et al.*, 2007] and could reflect subtle compositional variations across the range that are manifested in low U and Th concentrations in the samples presented in this study.

4.2. Analytical Methods: Apatite Fission Track Analysis

The same set of samples that was dated for AHe ages was also analyzed for AFT ages in the fission track laboratory at the University of Tübingen. Apatite grains were embedded in epoxy, ground, and polished to expose internal surfaces of the apatites. The apatite mounts were etched in 5.5 Mol HNO_3 for 20 s at 20°C to reveal the spontaneous tracks in apatite. Afterward, the mounts were covered with a 50 m thick uranium-free muscovite external detector and irradiated with thermal neutrons at the research reactor facility at Garching (FRM-II, Germany). After irradiation the external detectors were etched in 40% HF for 30 min to reveal the induced fission tracks. After etching, the external detector was placed back to its original position for track counting.

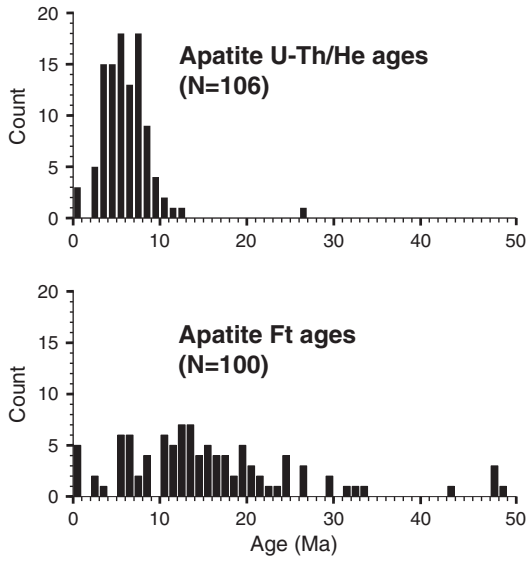

Figure 5. Measured age distribution of apatite cooling ages for both (top) the detrital apatite (U/Th)He ages and (bottom) detrital apatite fission track ages.

Spontaneous and induced fission tracks were counted at a nominal magnification of 1000X using a Zeiss Axioskope microscope, by focusing first at the apatite surface and then moving up into the surface of the external detector [*Jonckheere et al.*, 2003]. Confined fission track length measurements were not possible due to the low spontaneous track density. The analytical results of the bedrock samples are summarized in Table S3, and all single grain ages of the detrital sample are given in Table S4. The distribution of measured ages is shown in Figure 5.

4.3. Calculation of Age Probability Distributions (PDFs)

A predicted age distribution was calculated assuming uniform erosion across the catchment of the Tiedemann Glacier. The predicted PDF was created by convolution of the hypsometry of the study area using an ice-free DEM (Figure 3b) [*Clarke et al.*, 2009] and the measured age-elevation relationship (Figure 4). As was described in section 2 and shown in Figure 1, this predicted PDF

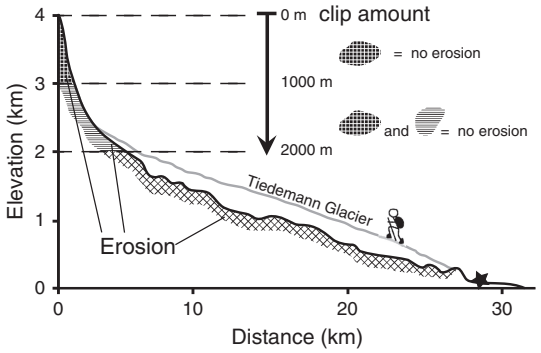

Figure 6. Schematic diagram of the distribution of subglacial erosion and how DEM clip amounts were used to generate revised elevation ranges of erosion in the Monte Carlo analysis. For a clip amount of 0 m the entire hypsometry contributed sediment to the analysis. For a clip amount of 1000 m erosion will start 1000 m beneath the summit (assuming no erosion contributing from the box-patterned area between 3 and 4 km). The background profile is the actual profile through the Tiedemann Glacier along the subglacial flow path (depicted in Figure 3b).

assumes every pixel of the DEM contributes equally to the age distribution and produces a smoothed distribution of the catchment hypsometric curve (Figure 3, inset). Afterward, a measured PDF was created using the grain age data of all acceptable ages described in section 4.2 (Figure 5) and the age-elevation relationship (Figure 4). The PDFs were generated following the approach of *Brandon* [1996] with an alpha value of 0.6 to avoid double smoothing of the stacked distributions. The Kuiper statistic tests described below were conducted on the continuous distribution functions (CDF) of each distribution.

Inspection of the measured PDFs provides information on the source elevation of the sediment and hence the distribution of erosion with elevation. However, quantifying the distribution of erosion is helped by the creation of additional predicted PDFs whereby different bands of elevation are systematically removed or "clipped" from the top elevation of the DEM (Figure 6). This approach of "clipping" elevations off the DEM assesses if erosion is focused in particular elevation bands in the landscape. While more complicated approaches for quantifying the distribution of erosion are possible (e.g., erosion as a function of basal sliding velocity or shear stress), the simplified approach of incremental clipping of elevations off the top of the DEM are used here because it has the fewest assumptions and free parameters. A new predicted PDF is created from the clipped DEM for comparison to the observed age PDF to test if the clipped elevation range could produce the observed ages. We created predicted PDFs for nine different clip amounts (Table 1) in 200 m intervals which were removed from the highest elevation considered in the model (4000 m), starting with 0 m (therefore including the entire elevation range of 530 m to 3960 m) to a maximum clip amount of 1600 m (only including elevations from 530 to 2400 m and thus the lower 1870 m of the catchment). These clip amounts define the range of elevations that the model uses

Table 1. Kuiper Statistical Test Results of Monte Carlo Simulations Comparing Predicted and Observed Distributions of Erosion[a]

	Apatite (U-Th)/He Data		Apatite Fission Track Data	
Clip Amount	% Different ($n = 106$)	% Different ($n = 50$)	% Different ($n = 100$)	% Different ($n = 50$)
0	1	0	100	100
200	1	0	100	100
400	1	0	100	100
600	1	0	100	100
800	1	0	100	100
1000	0	0	100	100
1200	0	0	100	100
1400	1	0	100	100
1600	10	1	100	100
1800	46	7	100	100
2000	94	32	100	100
2200	100	100	100	100
2400	100	100	100	100
2600	100	100	100	100

[a]Summary of PDF results based on the detrital AHe data. This table shows the nine clip amounts which were clipped off the top of the catchment, the corresponding total elevation considered in the model, and the average Kuiper test results for 10,000 model runs using all ($n = 106$) or 50 randomly selected data points ($n = 50$). The Kuiper test results shown have a 95% confidence level for different clip amounts. Where predicted and measured PDF are less than 5% different from each other, the Kuiper test is passed and the clip amount is possible. Model results of 0% difference from the measured PDF indicate statistically best results with the best fit at a clip amount of 200 m.

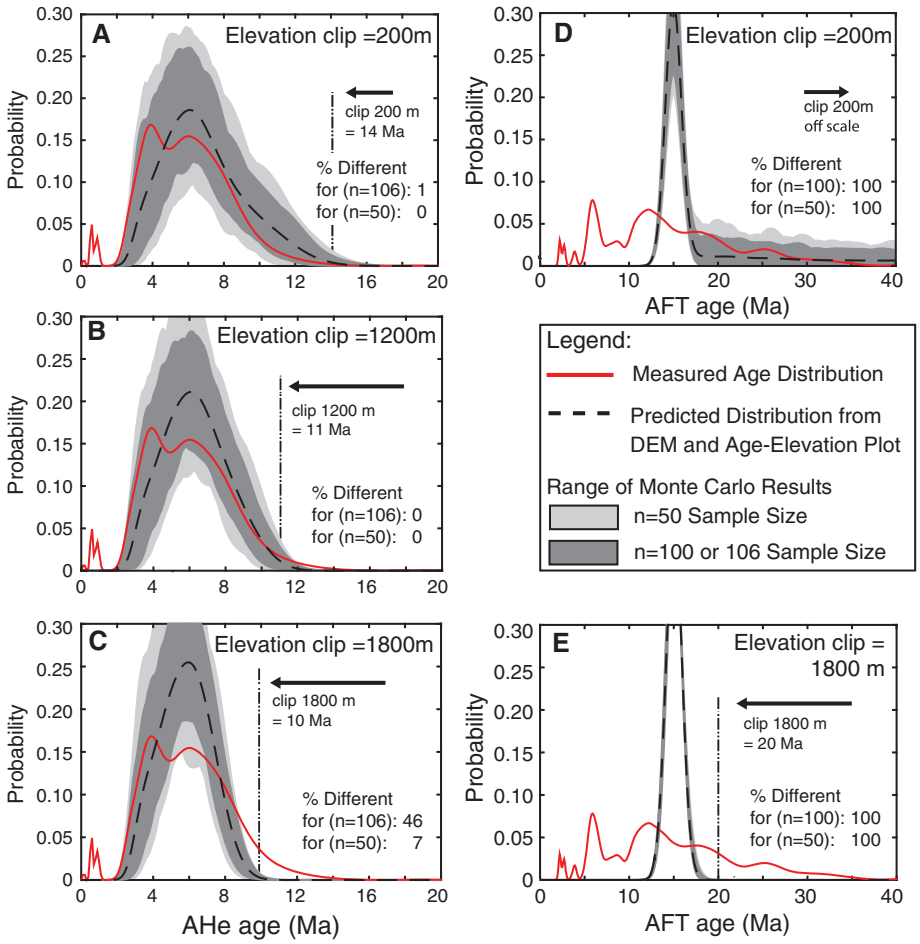

Figure 7. Results from the Monte Carlo analysis for predicted and observed grain age PDFs for three different DEM clip amounts for (a–c) the AHe and (d and e) AFT data. Probability density functions for the detrital sample 09TETG015. Red line shows the measured PDF of cooling ages. Light grey and dark grey envelopes show predicted probabilities for randomly grabbing 50 or using all 106 ages, respectively. The dashed curve shows an idealized predicted PDF if every pixel in the DEM contributed an apatite grain to the sample (uniform erosion assumption). Respective ages for clip amounts are indicated by vertical dash-dotted lines.

when calculating the probability of sediment delivery (Figure 6). For example, clipping the DEM from the top down results in only considering sediment sources from elevations between 530–3800 (for 200 m clip), 530–3600 (for 400 m clip), and so on until 530–2400 m (1600 m clip) is considered.

4.4. Monte Carlo Analysis

For each of these 14 clip amounts we performed a Monte Carlo analysis by repeating the process of constructing a synthetic distribution 10,000 times for sample sizes of $n = 50$ (for illustrative purposes) and $n = 106$ (the actual number of measured AHe ages). A Monte Carlo analysis is required because the actual number of grains measured is significantly less (by orders of magnitude) than the number of pixels in the DEM and the PDF sampling bias need to be evaluated. For example, 106 (for AHe) or 100 (for AFT) random pixels are selected from the DEM. For each selected pixel, we generate a normal distribution with a mean age based on the age-elevation relationship and a standard deviation based on the reproducibility of the bedrock ages. Finally, a value is randomly selected from each normal distribution to generate the synthetic grain age population that is compared to the measured age population and tested for statistical equality. This method acknowledges the reproducibility error in the measured ages by simulating this effect in the synthetic (predicted) distributions.

The range of predicted PDFs from the Monte Carlo analyses were combined and shown as grey shaded regions for the two different sample sizes (Figure 7) to identify the range of possible cooling age

distributions that could have been measured for each clip amount. The upper and lower limits of all generated possibilities encompass an envelope of possible curves that can be created with the data. We then compared each prediction of the Monte Carlo analysis for $n = 106$ (AHe) or $n = 100$ (AFT) to the measured age distribution. This comparison was done using a Kuiper equality test of the CDF for each distribution to ascertain if the two samples (the measured ages and the synthetic distribution) are different at the 95% confidence level (method after *Ruhl and Hodges* [2005] and *Stock et al*. [2006]). The Kuiper statistical test uses the maximum differences of the cumulative distribution functions of the two sample populations (measured versus synthetic) to calculate the test statistic. This quantifies the probability that the measured cooling age distributions are derived from a specific range of elevations in the catchment, while taking into account the uncertainty in ages and the range of elevations associated with that age uncertainty. The frequency at which the distributions are statistically different (at the 95% confidence interval) over the 10,000 Monte Carlo iterations is tracked to guide our interpretation on the distribution of erosion in the Tiedemann catchment. Results form the Kuiper tests of the Monte Carlo simulations are presented in Table 1.

5. Results

5.1. Observed Cooling Ages

The locations, ages, and 1σ errors for the bedrock samples are presented in Figure 3a. Most AHe ages increase with elevation (Figure 4). The range of bedrock AHe ages (~4–10 Ma over 2400 m relief) is similar to the AHe age-elevation profile reported by *Densmore et al*. [2007] (2.3–12 Ma over 2300 m relief) from ~40 km away on the west side of Mount Waddington. The bedrock AFT ages are also similar between the two studies. The similarity in the age-elevation relationships between the two studies separated by a large distance provides confidence that this relationship is robust within the significantly smaller catchment study area considered here and that the effects of faulting are minimal (see also section 6). The causes for deviations from this relationship could include spatially variable erosion magnitudes and rates within the catchment, topographic bending of isotherms and their effect on cooling ages, and/or small variations in deformation and erosion in the catchment in the last ~10 Ma. Concerning the later point—no evidence of recent faulting was visible in the catchment during sample collection or in previous work by the authors in the region [e.g., *Ehlers et al*., 2006]. Figure 3a shows all of the measured bedrock cooling ages, although only seven of the AHe ages were used to determine the age-elevation relationship used for the convolution with the hypsometry (Figure 1a). The bedrock data have 1σ reproducibility errors that range from 6.9 to 49.9% throughout the profile (Table S1). Samples 09TETG003 and 004 were excluded because of low gas yield from the samples. The resulting best fit linear regression for our age-elevation relationship has a slope of 0.31 km/Ma and a zero age depth (*y* intercept) at 266 m. This relationship was used to calculate our measured and predicted AHe PDFs.

The age-elevation plot of the AFT ages shows a typical exhumed partial annealing zone with much older ages at the highest elevations, whereby the ages below 2000 m elevation record a more rapid pulse of cooling at 16 ± 2 Ma (Figure 4). The break in slope evident in the AFT data suggests the presence of an exhumed partial annealing zone above ~2000 m. The ~2000 m elevation and timing of this break in slope are consistent with previous AFT data from the Mount Waddington region [*O'Sullivan and Parrish*, 1995] collected 50 km to the west of our study area. AFT ages from *O'Sullivan and Parrish* [1995] and this study (Figure 3) suggest exhumation rates changed in this region at ~14–16 Ma. Unfortunately, the near vertical age-elevation relationship in the AFT data below 2000 m elevation means that this data set is not sensitive to variations in erosion below this elevation. The large variation in ages above this elevation is potentially useful for determining the sediment source; however, only a small fraction of the catchment area is present at these elevations. These caveats to the AFT data are present in the detrital AFT ages presented below.

The distribution of measured detrital ages from the modern outwash of the glacier shows AHe ages ranging from 0.15 to 12.7 Ma, with two older grains at 25.4 and 98.5 Ma (Figure 5). The AHe age distribution indicates a large population between 3 and 10 Ma and three grains of <1 Ma. These <1 Ma grains suggest a possible source of very young ages somewhere in the catchment and cannot be explained by poor sample quality or analytical uncertainties. As expected from the age-elevation relationship of the bedrock samples, the detrital AFT age distribution is much larger and older than the AHe data with the main age population between 5 and 30 Ma. However, similar to the AHe age distribution there also exists a small population of

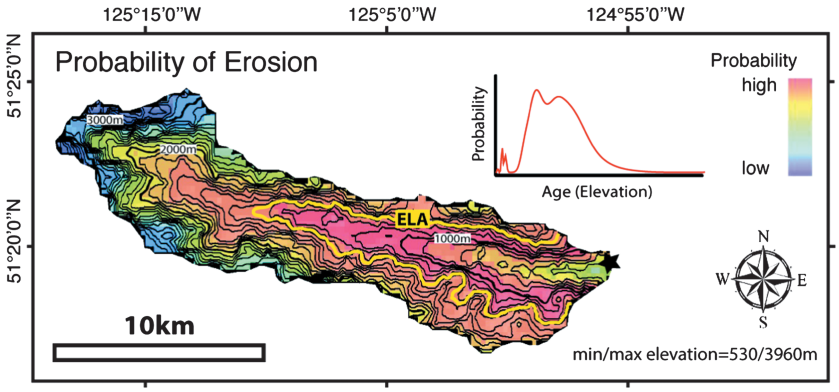

Figure 8. Observed probability of catchment erosion determined from the measured apatite (U–Th)/He grain age distribution mapped on to the ice-free DEM. Red areas (corresponding to elevations) have highest and blue lowest probability of eroding and thus delivering sediment to the sample location (star). The average single-grain uncertainty is 21% (determined from bedrock age reproducibility) of the measured detrital age and therefore results in elevation-dependent variations in the probability of erosion shown here. For example, uncertainties in the erosion shown here are ±100 m at 513 m elevation to ±620 m at 3960 m elevation. Yellow line marks the position of the ELA, determined after the technique described by *Leonard and Fountain* [2003].

very young (<3 Ma) AFT ages in the detrital age distribution (Figure 5). A significant fraction of the AFT ages is below 20 Ma. These cooling ages come from elevations below 2000 m where the AFT age-elevation is nearly uniform (Figure 4) and therefore cannot robustly determine the elevation source of each grain.

5.2. Monte Carlo Model Results

The Monte Carlo analysis was used to compare the measured and predicted distributions and to quantify the spatial distribution of erosion in the catchment. This procedure was repeated for both thermochronometer systems 14 different times each for clip amounts between 0 and 2600 m at 200 m increments (Figure 6 and Table 1). For each clip amount sample subsets of $n = 106$ (for AHe) and $n = 100$ (for AFT, total number of measured grains) and $n = 50$ grains (to avoid bias in the age distribution resulting from the limited number of grains) were randomly picked from the predicted distribution (hypsometry and age-elevation relationship derived) 10,000 times. This procedure was repeated for each clip amount and for the AHe and AFT thermochronometer systems for a total of 280,000 Monte Carlo simulations. Each of the 280,000 Monte Carlo realizations from the predicted distributions were compared to the measured ages using a Kuiper equality tests to determine if they are statistically identical at the 95% confidence level (Table 1). The 21% uncertainty in sample ages is used in this analysis such that the results presented below include the range of elevations associated with the age uncertainty.

Results from the Monte Carlo simulations for both $n = 50$ and $n = 106$ (or 100 for AFT data) grains and a wide range of clip amounts were found to produce a significant spatial variation in the statistically probable distribution of catchment erosion (Table 1). For the simulations using all 106 AHe measured ages, clip amounts between 0 and 1200 m produce a good fit to the data at the 95% confidence level indicating a $< 5\%$ difference between the predicted and observed PDFs (Figures 7a and 7b and Table 1). All clip amounts larger than this by far exceed the 5% difference limit of the Kuiper test (10%–100%) and thus represent improbable erosion distributions. The best fit Monte Carlo results (0% different) occur for DEM clip amounts between 1000 and 1200 m (e.g., Figure 7b), although a minimal difference (<1%) between predicted and observed grain age distributions is present for clip amounts between 0 and 1400 m from the top of the catchment (e.g., Figure 7a). For clip amounts larger than 1400 m the misfit between predicted and observed grain age distributions increases (e.g., Figure 7c). This result indicates focused erosion only at elevations below 1400 m from the top of the catchment are improbable. Taken together, our results suggest that erosion in the catchment is more or less uniform with a possibility of reduced erosion in the upper 1000–1200 m of the catchment. We emphasize that high-elevation, glacier-free regions of the catchment comprise a smaller fraction of the catchment area than do the ice-covered regions (Figure 3). Although our results suggest nearly uniform erosion, a larger fraction of sediment will be produced from under the ice-covered regions than above it because of the greater catchment area under the ice (see also discussion in Figure 8 below).

Monte Carlo analysis of predicted and observed AFT cooling age distributions is less insightful. For clip amounts between 0 and 2600 m elevation no statistically significant fits were found (Figures 7d and 7e and Table 1). For example, a 100% difference between all Monte Carlo simulations and observed ages was found for all clip amounts. Visual inspection in Figures 7d and 7e highlights that the majority of detrital AFT ages are sourced from elevations between 0 and 2000 m (or 0–20 Ma). The near vertical trend in the AFT age-elevation relationship at elevations below 2000 m prohibits a robust interpretation of the elevation this sediment was sourced from.

For comparison, the Monte Carlo simulations using only 50 randomly picked ages from the predicted distribution are also shown in Table 1 for both thermochronometer systems. Results indicate that a wider range of clip amounts (between 0 and 1800 m) produce a good fit (<10% different) to the data. Comparison of the larger ($n = 106$) and smaller number ($n = 50$) of grains in Table 1 highlights the utility of measuring more grains to define the elevation range erosion occurs over as suggested by *Vermeesch* [2004]. However, the preparation of AHe samples is both extremely time consuming and expensive such that more than ~100 analyses is often difficult.

6. Discussion

The Monte Carlo results (Figure 7) demonstrate that the cooling age PDFs allow for a wide elevation range of sediment sources in the Tiedemann Glacier catchment. In the following sections factors influencing the interpretation of glacial erosion from our data as well as erosion patterns that result from this study are discussed.

6.1. Factors Influencing the Interpretation of Detrital Thermochronometer Data

In addition to the factors discussed in *Stock et al*. [2006], we present six factors in our data set and study area that can influence the interpretation of the detrital data. First, as previously mentioned, the AHe bedrock samples have an average reproducibility error of 21% based on five to nine single-grain replicate analyses processed for each hand sample. The magnitude of this uncertainty influences the interpretation of the measured PDF by determining the "smoothness" of it. Higher uncertainties result in a smoother PDF and thereby inhibit a more detailed interpretation of the distribution of erosion at different elevations than if a low uncertainty is present. Ideally, for a bedrock sample, all replicates should give the same age, since the grains are all derived from the same rock and experienced an identical cooling history. The uncertainty from the bedrock data presented in this study is larger than the ~9–11% uncertainty in previous AHe studies ~40 km to the west in similar igneous lithologies [e.g., *Ehlers et al*., 2006; *Densmore et al*., 2007]. The higher uncertainty reported here does not result from analytical or measurement errors. Almost all bedrock replicate samples were measured within hours of each other and variations in machine sensitivity (e.g., from temperature or humidity changes) are not a factor. Furthermore, all grain ages used have measured He, U, and Th well above blank levels (Table S1), and whole, to nearly whole, apatite grains were picked and analyzed meaning that the effects of measuring broken grains are likely not a factor [e.g., *Brown et al*., 2013; *Beucher et al*., 2013]. This leaves us to conclude, somewhat unsatisfactorily, that variations in grain age reproducibility are due to natural variability in the samples that could result from a suite of factors such as intergrain variations in diffusion kinetics, helium implantation from neighboring minerals in the rock, or hydrothermal alteration of grains and modification of the U, Th content. None of these factors can be verified as a source of the 21% reproducibility error with currently available data.

Second, it should be pointed out that a similar reproducibility error might adhere to the detrital grain age data. Because of the detrital nature of the sample (i.e., the grains being separated from their bedrock origin by erosion and being transported and mixed by water, wind, and ice), there is no way of determining the reproducibility for individual detrital ages. We can only measure a grain once and not compare the age to others that might have originated from a similar location.

Third, deviations in the bedrock AHe ages from the linear regression (Figure 4) could be the result of the topographic bending of isotherms over the distance where samples were collected from (Figure 1). Previous work has determined that topography with sufficient wavelength and amplitude can bend subsurface closure temperature isotherms to mimic the topography [e.g., *Lees*, 1910; *Stüwe et al*., 1994; *Braun*, 2005; *House et al*., 1998]. This effect would cause spatial variations in near-surface thermal gradients

and closure temperature depths. If AHe samples cooled through the closure temperature after development of topography, then the topographic bending of isotherms could cause the deviations in ages from the linear regression shown in Figure 4. The variations in closure temperature depth are problematic for the assumption of horizontal isotherms and a linear cooling age-elevation relationship [e.g., *Ehlers*, 2005; *Ehlers and Farley*, 2003], which is used in this study. Only if sample cooling significantly predates the formation of topography [e.g., *Stock et al*., 2006] can horizontal isotherms be assumed. The previous discussion implies that some to all of the deviations in our observed ages from the linear regression in Figure 4 represent topographic effects on the cooling ages. Correction for the topographic effect on closure isotherms requires application of detailed 3-D thermal models which is beyond the scope of this study because it would require consideration of how the topography has evolved during sample cooling [e.g., *Ehlers et al*., 2006; *Olen et al*., 2012]. Finally, it should also be noted that the deviation of ages from an expected linear age-elevation relationship could result from unknown spatial variations in erosion rates or recent (last 10–15 Ma) variations in deformation in the catchment area. Testing the previous hypotheses of topographic development and/or changes in exhumation rate influencing cooling ages is well beyond the scope of this study, and future modeling studies will address these considerations in detail. Instead, in this study we accept that this effect is present and close to the 21% reproducibility error in each sample and that the linear regression through the data (Figure 4) in effect minimizes the misfit between sample ages at different elevations. Furthermore, the extrapolation of the linear regression for the age-elevation relationship above the elevation of the highest measured bedrock sample (2651 m) poses a potential problem. Because the maximum catchment elevation reaches 3960 m, the age-elevation relationship for the upper 1300 m of the catchment can only be estimated based on the linear regression of the lower elevation samples. A potential change in gradient of this regression at higher elevations, which could indicate changes in exhumation rates or even a partial retention zone, could alter the interpretation of our PDF results. However, previous studies such as *Ehlers et al*. [2006] have documented apatite (U/Th)He ages between 12 Ma and 14 Ma at high elevations near the top of Mount Tiedemann and Mount Waddington. These locations lie within our catchment and the ages fit the regression used for this study, making the assumption of a linear, nonchanging age-elevation relationship acceptable.

Fourth, in this study we observed detrital AHe and AFT ages that are younger than the bedrock cooling age at the lowest sample elevation. Three detrital grains yielded AHe ages younger than 2 Ma, and five detrital grains have zero spontaneous fission tracks. These grains could be younger than the lowest elevation bedrock samples for reasons explained in the previous paragraphs, or they could indicate inaccuracies in the ice-free DEM used. For example, overdeepening of the glacial valley upstream of the detrital sample location could result in elevations lower than the sample elevation and explain the young ages. The ice-free DEM (Figure 3b [from *Clarke et al*., 2009]) did not show signs of overdeepening and was constructed using an artificial neural network which applied input data from neighboring formerly glaciated valleys to estimate the subice surface topography. It is possible that overdeepening hidden by the ice of the glacier could exist and could not be resolved by this approach. However, this explanation seems unlikely for two reasons. First, the modeled subglacial surface of the Tiedemann Glacier is remarkably straight and ramp like (Figure 6) with no major tributary glaciers joining it that could cause an overdeepening [e.g., *MacGregor et al*., 2000]. It is therefore difficult to envision enough ice accumulating to significantly increase erosion and form a large overdeepening. Second, according to the age-elevation relationship this overdeepening would have to incise more than 700 m, down to almost 200 m below sea level, to produce the youngest detrital age of 0.15 Ma. While this magnitude of overdeepening is quite large, it is plausible given the proximity to deep fjords in the region. Unfortunately, it is difficult to test this with existing data. One final explanation for the young ages could be recent volcanic or hydrothermal processes in the catchment. However, so far no evidence of such processes has been observed in this catchment.

The fifth factor worth mentioning concerning the interpretation of detrital thermochronometer data for glacial erosion is the presence or absence of a partial annealing or partial retention zone within the catchment. The bedrock AHe age-elevation relationship (Figure 4) reasonably approximates a linear relationship and does not indicate the presence of a partial retention zone. This implies that the method presented in Figures 1a and 1c is appropriate for this data set. However, the bedrock AFT data indicates the presence of an AFT partial annealing zone within the catchment. A large variation in ages with elevation is useful for determining the source elevation of sediment. Unfortunately, sample cooling ages

within a partial annealing zone can be highly variable and nonlinear with elevation from variations in annealing kinetics that influence cooling ages. Because of this, it is problematic to apply the technique shown in Figures 1a and 1c to this sample for elevations >2000 m where the PAZ is located. As previously discussed, the AFT data are nearly uniform at elevations <2000 m and therefore not useful as a sediment tracer. We therefore refrain in this study from interpreting the distribution of erosion from the AFT data and instead highlight this complexity and also that the detrital AFT peak in cooling ages at ~10–14 Ma (Figure 5) is consistent with the peak in AHe ages of ~5–8 Ma. Both these ages occur at the same elevation range (Figure 4) and suggest that the maximum amount of sediment is sourced from this area (see also next section).

Finally, active glacial systems can be complex in terms of where and how long sediment from different elevations is stored within the catchment. For example, cirques and lateral moraines can temporarily trap sediment that was sourced from higher elevations and retard its delivery to the outwash channel. The residence time of the sediments in these locations is not known and not quantifiable with our approach. However, mass wasting events from higher elevation can provide rock and sediment that bypasses these traps and makes it onto the glacier where it is transported [e.g., *Ward and Anderson*, 2011]. The previous sediment traps and mass wasting processes are not at this time something that can be quantified with this technique. Rather, our approach documents the integrated distribution of elevations within the catchment that sediment was produced from. Catchments with a larger range of cooling ages in the bedrock age-elevation profile coupled with thermochronometer sampling of individual deposits (e.g., lateral and terminal moraines) and different grain sizes holds potential to quantify subcatchment-scale processes, particularly if coupled with process-based models.

6.2. Distribution of Erosion From Apatite (U-Th)/He Data

In spite of the previous caveats (section 6.1) related to the interpretation of detrital data, the AHe data do allow for an approximation of the distribution of where sediment is sourced from in the Tiedemann Glacier catchment. To illustrate the catchment erosion pattern implied from our detrital age distribution, the results of the measured PDF are shown in map view on the ice-free catchment DEM (Figure 8). This map displays the probability of erosion versus the corresponding elevation over the catchment. This figure was generated by assigning colors ascending from blue to red to the probability range of the measured PDF (Figure 8, inset). Each elevation of the ice-free DEM was colored according to the probability (color) given by this curve. The 21% average uncertainty in ages results in an elevation-dependent uncertainty for the elevations shown (see figure caption for details).

Based on the technique described by *Leonard and Fountain* [2003] which uses changes in shape of supraglacial contour lines from concave to convex, the equilibrium line altitude (ELA) of the Tiedemann Glacier can be estimated between 1320 m and 1360 m. Because of the increased presence of liquid water below the ELA, it is expected that there is a larger amount of sediment from elevations near and below this line. This concurs with the lower end of the 1200 m to 1800 m elevation range of the maximum probability of elevations where sediment is sourced from (Figure 8). Moreover, Figure 8 shows that little to no sediment is sourced from predominantly ice-free elevations higher than 3000 m elevation (blue colors). These areas, as shown in Figure 3, are without significant present-day ice cover and thus not presently exposed to glacial erosion. They also comprise a smaller fraction of the catchment areas compared to the ice-covered region. Therefore, these higher elevations most likely do not contribute significant amounts of sediment from rock fall onto the glacier to the outwash where the detrital ages were measured. Furthermore, elevations near the terminus of the glacier (530–650 m) near the detrital sample location (star) also show a low probability of sediment sourced from these elevations (yellow and green colors). This finding is consistent with previous work by *Alley et al.* [2003] who showed that under certain conditions, glaciers can accumulate ground moraines near their terminus instead of discharging the sediment into terminal moraines or outwash planes. This occurs from a "supercooling" mechanism, which depends on the angles of the ice-air and ice-ground surfaces of the glacier. This phenomenon could explain the lack of sediment from these low elevations in our detrital sample and even point to subglacial sedimentation near the terminus.

Another factor to consider in interpreting thermochronometer age distributions from modern glacial outwash is glacial retreat over the past few decades [*Dyurgerov and Meier*, 2000]. This retreat is consistent

with an expanding wet-based portion of the glacier to higher elevations (and therefore older ages). Glacier responses to perturbations are on the order of multiple decades [*Oerlemans*, 1994] suggesting that the Tiedemann is in a state of transience due to recent climate change. This means that active subglacial sliding and meltwater flushing are reaching higher elevations than might be suggested by the current glacial extent; therefore, the measured distribution of ages may cover a wider elevation range than one might expect if the glacier was in equilibrium with the climate.

6.3. Hypothesis Evaluation and Future Potential

Our idealized concept for nonuniform erosion shown in Figure 1c has two distinct peaks and provides a graphical representation of the hypothesis evaluated in this study. Nonuniform erosion could result from glacial abrasion or plucking producing focused erosion at certain elevations in the catchment, or from large inputs of debris into the glacier from mass wasting events triggered at high elevations. Our measured distribution of ages contains two peaks (e.g., Figure 7a) and is suggestive of point sources in erosion, but they are nearly similar in age and cannot resolve the concept illustrated in Figure 1c when the age uncertainties are included in the Monte Carlo analysis. The lack of distinct local peaks of erosion in the Tiedemann catchment can be explained by the simple, ramp-like geometry of the valley topography. Without significant confluences of glaciers and steps in the topography such peaks in the age distribution may be difficult to produce.

This result seemingly falsifies our original hypothesis that detrital thermochronology can quantify nonuniform erosion in glaciated catchments. However, there are two important considerations to keep in mind. First, the results from the Monte Carlo analysis suggest that a best fit to data occurs with a clip amount between 1000 and 1200 m (Figure 7b and Table 1), meaning that there is slight preference for erosion occurring at lower elevations in the catchment, suggestive of a more diffuse pattern of nonuniform erosion than shown Figure 1c. Second, the detrital thermochronometer data presented in this catchment have a higher uncertainty (21%) than previous work we conducted in neighboring regions to the Tiedemann Glacier (~9–11%) [e.g., *Densmore et al*., 2007; *Ehlers et al*., 2006]. The higher uncertainties in the Tiedemann catchment coupled with a somewhat small age variation with elevation (Figure 4) prohibit a more detailed analysis of the data than is presented here. The analysis here could be improved with significantly more analyses of bedrock aliquots (e.g., ~ 20 aliquots per sample) so that statistical criteria for outliers could be applied to decrease the uncertainty used in the model analysis. If additional outliers in our bedrock samples could be objectively and rigorously identified, then other techniques such as calculation of a mean square weighted deviation for the bedrock aliquots could be applied and would result in decrease in grain age dispersion. This approach would increase the sensitivity of the detrital PDF (Figure 7, red line) to spatial variations in erosion. Thus, future application of the techniques presented here hold promise for a more detailed interpretation of glacial catchment erosion when the above factors are taken into consideration. The required conditions for this are that the samples have lower uncertainties, and a larger variation in bedrock ages is observed with increased elevation.

7. Summary and Conclusion

The subglacial erosion pattern of the Tiedemann Glacier documented by this study shows that detrital apatite (U/Th)-He ages from glacial sediments provide a new tool for analyzing glacial erosion processes. We have demonstrated that significant sediment is sourced mainly below an elevation of approximately 3000 m within the Tiedemann Glacier catchment in British Columbia, with the maximum amount of sediment coming from elevations between 1200 m and 1800 m (Figure 8). Both the nonglaciated areas at elevations above 3000 m and subglacial elevations below 650 m do not contribute much sediment to the glacial outwash. Results from a Monte Carlo model of the AHe data suggest nearly uniform erosion in the catchment, with a preference for sediment being sourced from ~2900 to 2700 m elevation. The quality of the Monte Carlo model results has proven to strongly depend on reproducibility of the bedrock data and the number of grains measured. Our analysis showed that larger sample quantities (when possible), lower uncertainties in bedrock sample reproducibility, and larger variation in ages with elevation could help further narrow and define erosion patterns. Despite these limitations, the method shown here demonstrates promise for quantifying patterns of glacial catchment erosion for other regions.

Acknowledgments

Garry Clarke is thanked for providing access to the ice-free DEM used in our analysis. We thank Des Patterson and ASI-Alphachron for their continued support of the Universität Tübingen gas extraction line. White Saddle Air provided helicopter support for sample collection. Greg Stock, Margi Rusmore, and Kenneth Farley are thanked for thought-provoking discussions over the years concerning the Coast Mountains Geology and detrital AHe thermochronometry. This research was partially supported by the German Deutsche Forschungsgemeinschaft (DFG) grant EH329/1-1 (to Ehlers). We thank James Spotila, Johnny Sanders, Pieter Vermeesch, Simon Brockelhurst, Byron Adams, an anonymous reviewer, and Alex Densmore for thoughtful comments that improved this manuscript.

References

Alley, R. B., D. E. Lawson, G. J. Larson, E. B. Evenson, and G. S. Baker (2003), Stabilizing feedbacks in glacier bed erosion, *Nature*, *424*, 758–760.

Anderson, R. S., P. Molnar, and M. A. Kessler (2006), Features of glacial valley profiles simply explained, *J. Geophys. Res.*, *111*, F03013, doi:10.1029/2005JF000334.

Avdeev, B., N. A. Niemi, and M. K. Clark (2011), Doing more with less: Bayesian estimation of erosion models with detrital thermochronometric data, *Earth Planet. Sci. Lett.*, *305*, 385–395.

Berger, A. L., et al. (2008), Quarternary tectonic response to intensified glacial erosion in an orogenic wedge, *Nat. Geosci.*, *1*, 793–799, doi:10.1038/ngeo334.

Beucher, R., R. W. Brown, S. Roper, F. Stuart, and C. Persano (2013), Natural age dispersion arising from the analysis of broken crystals: Part II. Practical application to the apatite (U-Th)/He thermochronometry, *Geochim. Cosmochim. Acta*, *120*, 395–416, doi:10.1016/j.gca.2013.05.042.

Brandon, M. T. (1996), Probability density plot for fission-track grain-age samples, *Radiat. Meas.*, *26*, 663–676.

Braun, J. (2005), Quantitative constraints on the rate of landform evolution derived from low-temperature thermochronology, *Rev. Mineral. Geochem.*, *58*, 351–374, doi:10.2138/rmg.2005.58.13.

Braun, J., D. Zwartz, and J. H. Thomkin (1999), A new surface-processes model combining fluvial and glacial erosion, *Ann. Glaciol.*, *28*, 282–290.

Brewer, I. D., D. W. Burbank, and K. V. Hodges (2003), Modelling detrital cooling-age populations: Insights from two Himalayan catchments, *Basin Res.*, *15*, 305–320.

Brodzikowski, K., and A. J. van Loon (1991), *Developments in Sedimentology 49: Glacigenic Sediments*, pp. 673, Elsevier, New York.

Brown, R. W., R. Beucher, S. Roper, C. Persano, F. Stuart, and P. Fitzgerald (2013), Natural age dispersion arising from the analysis of broken crystals: Part I. Theoretical basis and implications for the apatite (U-Th)/He thermochronometer, *Geochim. Cosmochim. Acta*, *122*, 478–497, doi:10.1016/j.gca.2013.05.041.

Carlson, W. D., R. A. Donelick, and R. A. Ketcham (1999), Variability of apatite fission track annealing kinetics: I. Experimental results, *Am. Mineral.*, *84*, 1213–1223.

Carrapa, B., M. R. Strecker, and E. R. Sobel (2006), Cenozoic orogenic growth in the central Andes: Evidence from sedimentary rock provenance and apatite fission track thermochronology in the Fiambalá Basin, southernmost Puna Plateau margin (NW Argentina), *Earth Planet. Sci. Lett.*, *247*, 82–100.

Carter, A. (1999), Present status and future avenues of source region discrimination and characterization using fission-track analysis, *Sediment. Geol.*, *124*, 31–45.

Clarke, G., E. Berthier, C. G. Schoof, and A. H. Jarosch (2009), Neural networks applied to estimating subglacial topography and glacier volume, *J. Clim.*, *22*, 2146–2160.

Densmore, M. S., T. A. Ehlers, and G. J. Woodsworth (2007), Effect of Alpine glaciation on thermochronometer age-elevation profiles, *Geophys. Res. Lett.*, *34*, L02502, doi:10.1029/2006GL028371.

Dyurgerov, M. B., and M. F. Meier (2000), Twentieth century climate change: Evidence from small glaciers, *Proc. Natl. Acad. Sci. U.S.A.*, *97*, 1406–1411, doi:10.1073/pnas.97.4.1406.

Egholm, D. L., S. B. Nielsen, V. K. Pedersen, and J.-E. Lesemann (2009), Glacial effects limiting mountain height, *Nature*, *460*, 884–887.

Ehlers, T. A. (2005), Crustal thermal processes and thermochronometer interpretation, *Rev. Mineral. Geochem.*, *58*, 315–350.

Ehlers, T. A., and K. A. Farley (2003), Apatite (U-Th)/He thermochronometry: Methods and applications to problems in tectonic and surface processes, *Earth Planet. Sci. Lett.*, *206*, 1–14.

Ehlers, T. A., K. A. Farley, M. Rusmore, and G. J. Woodsworth (2006), Apatite (U-Th)/He signal of large-magnitude accelerated glacial erosion, southwest British Columbia, *Geology*, *34*, 765–768.

Enkelmann, E., and T. A. Ehlers (2013), Evaluation of detrital apatite fission track thermochronology for quantification of glacial catchment denudation and sediment mixing, Abstract T43F-2723 presented at 2013 Fall Meeting, AGU, San Francisco, Calif., 9–13 Dec.

Enkelmann, E., P. K. Zeitler, T. L. Pavlis, J. I. Garver, and K. D. Ridgway (2009), Intense localized rock uplift and erosion in the St Elias orogeny of Alaska, *Nat. Geosci.*, *2*, 360–363, doi:10.1038/ngeo502.

Farley, K. A. (2000), Helium diffusion from apatite: General behavior as illustrated by Durango fluorapatite, *J. Geophys. Res.*, *105*(B2), 2903–2914, doi:10.1029/1999JB900348.

Farley, K. A. (2002), (U-Th)/He dating: Techniques, calibrations, and applications, *Rev. Mineral. Geochem.*, *47*, 819–844.

Farley, K. A., R. A. Wolf, and L. T. Silver (1996), The effects of long stopping distances on (U-Th)/He ages, *Geochim. Cosmochim. Acta*, *60*(21), 4223–4229.

Goodsell, B., M. J. Hambrey, and N. F. Glasser (2005), Debris transport in a temperate valley glacier: Haut Glacier d'Arolla, Valais, Switzerland, *J. Glaciol.*, *51*, 139–146.

Green, P. F., I. R. Duddy, A. J. W. Gleadow, P. T. Tingate, and G. M. Laslett (1986), Thermal annealing of fission tracks in apatite: 1. A qualitative description, *Isot. Geosci.*, *59*, 237–253.

Hallet, B., L. Hunter, and J. Bogen (1996), Rates of erosion and sediment evacuation by glaciers: A review of field data and their implications, *Global Planet. Change*, *12*, 213–235.

Hambrey, M. J., M. R. Bennett, J. A. Dowdeswell, N. F. Glasser, and D. Huddart (1999), Debris entrainment and transfer in polythermal valley glaciers, *J. Glaciol.*, *45*, 69–86.

Headley, R. M., and T. A. Ehlers (2015), Ice flow models and glacial erosion over multiple glacial-interglacial cycles, *Earth Surf. Dyn.*, *3*, 153–170, doi:10.5194/esurf-3-153-2015.

Herman, F., and J. Braun (2008), Evolution of the glacial landscape of the Southern Alps of New Zealand: Insights from a glacial erosion model, *J. Geophys. Res.*, *113*, F02009, doi:10.1029/2007JF000807.

Herman, F., D. Seward, P. Valla, A. Carter, B. Kohn, S. D. Willett, and T. A. Ehlers (2013), Worldwide acceleration of mountain erosion under a cooling climate, *Nature*, *504*, 423–426, doi:10.1038/nature12877.

House, M. A., B. P. Wernicke, and K. A. Farley (1998), Dating topography of the Sierra Nevada, California, using apatite (U–Th)/He ages, *Nature*, *396*, 66–69, doi:10.1038/23926.

Hurford, A. J., and A. Carter (1991), The role of fission track dating in discrimination of provenance, in *Developments in Sedimentary Provenance Studies*, edited by A. C. Morton, S. P. Todd, and P. D. W. Haughton, *Geol. Soc. London Spec. Publ.*, *57*, 67–78.

Jonckheere, R., L. Ratschbacher, and G. A. Wagner (2003), A repositioning technique for counting induced fission tracks in muscovite external detectors in single-grain dating of minerals with low and inhomogeneous uranium concentrations, *Radiat. Meas.*, *37*, 217–219.

Kuhlemann, J., I. Dunkl, A. Brügel, C. Spiegel, and W. Frisch (2005), From source terrains of the Eastern Alps to the Molasse Basin: Detrital record of non-steady-state exhumation, *Tectonophysics*, *413*, 301–316.

Laroque, S. J., and D. J. Smith (2003), Little Ice Age glacial activity in the Mt. Waddington area, British Columbia, Coast Mountains, Canada, *Can. J. Earth Sci.*, *40*, 1413–1436.
Laroque, S. J., and D. J. Smith (2005), Little Ice Age proxy glacier mass balance records reconstructed from tree rings in the Mt Waddington area, British Columbia, Coast Mountains, Canada, *Holocene*, *15*, 748–757.
Lees, C. H. (1910), On the isogeotherms under mountain ranges in radioactive districts, *Proc. Roy. Soc.*, *83*, 339–346.
Leonard, K. C., and A. G. Fountain (2003), Map-based methods for estimating glacier equilibrium-line altitudes, *J. Glaciol.*, *49*, 329–336.
MacGregor, K. R., R. S. Anderson, S. P. Anderson, and E. D. Waddington (2000), Numerical simulations of glacial-valley longitudinal profile evolution, *Geology*, *28*(11), 1031–1034.
McDougall, I., and T. M. Harrison (1999), *Geochronology and Thermochronology by the $^{40}Ar/^{39}Ar$ Method*, 267 pp., Oxford Univ. Press, New York.
McPhillips, D., and M. T. Brandon (2010), Using tracer thermochronology to measure modern relief change in the Sierra Nevada California, *Earth Planet. Sci. Lett.*, doi:10.1016/j.epsl.2010.05.022.
Menzies, J., and W. W. Shilts (2002), Subglacial environments, in *2002 Modern and Past Glacial Environments*, edited by J. Menzies, pp. 183–278, Butterworth-Heinemann, Oxford.
O'Sullivan, P. B., and R. R. Parrish (1995), The importance of apatite composition and single-grain ages when interpreting fission track data from plutonic rocks: A case study from the Coast Ranges, British Columbia, *Earth Planet Sci. Lett.*, *132*(1–4), 213–224.
Oerlemans, J. (1994), Quantifying global warming from the retreat of glaciers, *Science*, *264*(5156), 243–245, doi:10.1126/science.264.5156.243.
Olen, S., T. A. Ehlers, and M. Densmore (2012), Limits to reconstructing paleotopography from thermochronometer data, *J. Geophys. Res.*, *117*, F01024, doi:10.1029/2011JF001985.
Osborn, G., and B. H. Luckman (1988), Holocene glacier fluctuations in the Canadian Cordillera (Alberta and British Columbia), *Quat. Sci. Rev.*, *7*, 115–128.
Parrish, R. (1983), Cenozoic thermal evolution and tectonics of the Coast Mountains of British Columbia: 1. Fission track dating, apparent uplift rates, and patterns of uplift, *Tectonics*, *2*, 601–631, doi:10.1029/TC002i006p00601.
Reiners, P. W., S. N. Thomson, D. McPhillips, R. A. Donelick, and J. J. Roering (2007), Wildfire thermochronology and the fate and transport of apatite in hillslope and fluvial environments, *J. Geophys. Res.*, *112*, F04001, doi:10.1029/2007JF000759.
Ruhl, K. W., and K. V. Hodges (2005), The use of detrital mineral cooling ages to evaluate steady-state assumptions in active orogens: An example from the central Nepalese Himalaya, *Tectonics*, *24*, TC4015, doi:10.1029/2004TC001712.
Rusmore, M. E., and G. J. Woodsworth (1994), Evolution of the eastern Waddington thrust belt and its relation to the mid-Cretaceous Coast Mountains arc, western British Columbia, *Tectonics*, *13*, 1052–1067, doi:10.1029/94TC01316.
Schaller, M., F. von Blanckenburg, N. Hovius, and P. W. Kubik (2001), Large-scale erosion rates from in situ-produced cosmogenic nuclides in European river sediments, *Earth Planet. Sci. Lett.*, *188*, 441–458.
Shuster, D., T. A. Ehlers, M. Rusmore, and K. Farley (2005), Rapid glacial erosion at 1.8 Ma revealed by $^{4}He/^{3}He$ thermochronometry, *Science*, *310*, 1668–1670.
Spiegel, C., W. Siebel, J. Kuhlemann, and W. Frisch (2004), Towards a comprehensive provenance analysis: A multi-method approach and its implications for the evolution of the Central Alps, in *Detrital Thermochronology—Provenance Analysis, Exhumation, and Landscape Evolution of Mountain Belts*, GSA Spec. Publ., vol. 378, edited by M. Bernet and C. Spiegel, pp. 37–50, Boulder, Colo.
Stock, G., T. A. Ehlers, and K. Farley (2006), Where does sediment come from? Quantifying catchment erosion with detrital apatite (U-Th)/He thermochronometry, *Geology*, *34*, 725–728.
Stüwe, K. L., L. White, and R. Brown (1994), The influence of eroding topography on steady-state isotherms: Application to fission track analysis, *Earth Planet Sci. Lett.*, *124*, 63–76.
Tranel, L. M., J. A. Spotila, M. J. Kowalewski, and C. M. Waller (2011), Spatial variation of erosion in a small, glaciated basin in the Teton Range, Wyoming, based on detrital apatite (U-Th)/He thermochronology, *Basin Res.*, *23*, 571–590, doi:10.1111/j.1365-2117.2011.00502.x.
Tripathy-Lang, A., K. V. Hodges, B. D. Monteleone, and M. C. van Soest (2013), Laser (U-Th)/He thermochronology of detrital zircons as a tool for studying surface processes in modern catchments, *J. Geophys. Res. Earth Surf.*, *118*, 1333–1341, doi:10.1002/jgrf.20091.
Vermeesch, P. (2004), How many grains are needed for a provenance study?, *Earth Planet. Sci. Lett.*, *224*, 441–451.
Vermeesch, P. (2007), Quantitative geomorphology of the White Mountains (California) using detrital apatite fission track thermochronology, *J. Geophys. Res.*, *112*, F03004, doi:10.1029/2006JF000671.
Vermeesch, P., D. Avigad, and M. O. Mc Williams (2009), 500 m.y. of thermal history elucidated by multi-method detrital thermochronology of North Gondwana Cambrian sandstone (Eliat area, Israel), *Bull. Geol. Soc. Am.*, *121*, 1204–1206.
Ward, D. J., and R. S. Anderson (2011), The use of ablation-dominated medial moraines as samplers for ^{10}Be-derived erosion rates of glacier valley walls, Kichatna Mountains, AK, *Earth Surf. Processes Landforms*, *36*, 495–512.
Whipp, D. M., Jr., T. A. Ehlers, J. Braun, and C. D. Spath (2009), Effects of exhumation kinematics and topographic evolution on detrital thermochronometer data, *J. Geophys. Res.*, *114*, F04014, doi:10.1029/2008JF001195.
Yanites, B. J., and T. A. Ehlers (2012), Global climate and tectonic controls on the denudation of glaciated mountains, *Earth Planet. Sci. Lett.*, *325–326*, 63–75, doi:10.1016/j.epsl.2012.01.030.